Molecular Crystals and Liquid Crystals

Publication details, including instructions for authors and subscription information:
http://www.tandfonline.com/loi/gmcl20

Dynamic ^{1}H NMR Investigation of the Liquid Crystal MBBA Confined in Porous Silica

R. Decressain [a], T. Mansare [a], C. Gors [a], E. Cochin [a] & L. Carpentier [a]

[a] Laboratoire de Structure et Dynamique Des Materiaux Moleculaires (LDSMM), University of Lille-1, Villeneuve d'Ascq, France

Version of record first published: 20 Dec 2006

To cite this article: R. Decressain, T. Mansare, C. Gors, E. Cochin & L. Carpentier (2006): Dynamic ^{1}H NMR Investigation of the Liquid Crystal MBBA Confined in Porous Silica, Molecular Crystals and Liquid Crystals, 460:1, 43-61

To link to this article: http://dx.doi.org/10.1080/15421400600700398

Mol. Cryst. Liq. Cryst., Vol. 460, pp. 43–61, 2006

ISSN: 1542-1406 print/1563-5287 online
DOI: 10.1080/15421400600700398

Taylor & Francis
Taylor & Francis Group

Dynamic ^{1}H NMR Investigation of the Liquid Crystal MBBA Confined in Porous Silica

R. Decressain
T. Mansare
C. Gors
E. Cochin
L. Carpentier
Laboratoire de Structure et Dynamique Des Materiaux Moleculaires (LDSMM), University of Lille-1, Villeneuve d'Ascq, France

The polymorphism and molecular dynamics of the liquid crystal MBBA [N-(p-methoxybenzylidene)-p-n-butylaniline], confined in controlled pores glasses (CPG) porous glasses of 82, 156, and 337 Å pore diameter, were investigated using ^{1}H nuclear magnetic resonance spectroscopy (NMR). The transition temperatures are determined from the analysis of NMR line-shapes and spin-lattice relaxation times (T_1). The results show that the depression of the phase-transition temperatures is linear versus inverse pore diameter. The motion parameters of the phases were derived from an isotropic rotational diffusion model (BPP). In the nematic and glassy nematic phases, the results show that the confinement weakly influences the dynamics. In the crystalline phases, the confinement results in a reduction of the motion activation energies and an important phase diagram modification. To interpret the experimental results with regard to the bulk characteristics properties, a Cole–Cole distribution model was introduced. The width distribution parameter was found to depend linearly on the inverse pore diameter in the crystalline phases.

Keywords: confined; liquid crystal; NMR

1. INTRODUCTION

The investigations of confined materials have received a considerable amount of attention from both theoretical and experimental researchers [1–21]. It is now well established that materials confined in pores can exhibit physical and chemical properties that are different from the bulk properties. By thermal investigations, it has been observed

Address correspondence to Regis Decressain, LDSMM, CNRS UMR 8024, Université de Lille-1, Villeneuve d'Ascq, 59655, France. E-mail: regis.decressain@univ-lillel.fr

that the melting and freezing phase transitions are broadened and occur at temperatures different from those of the bulk. The difference between the bulk and confined melting point ΔT_m is generally interpreted by the Gibbs–Thomson equation [16,17]. According to this model, ΔT_m is proportional to the reverse pore diameter (d): $\Delta T_m = T_m - T_m(d) = K/d$, where $\Delta T_m(d)$ is the freezing point of crystals of size d and K is a material specific constant. The value of ΔT_m depends on the interaction between the pore wall and the confined material via the constant K in the Gibbs–Thomson equation. This model, which has been successively applied in liquids confined in spherical or cylindrical cavities, does not hold for very small pores because surface heterogeneities and finite size effects are not taken into account. In recent years, confined liquid crystals (LCs) have been extensively investigated to understand the possible disappearance of the nematic phase when they are strongly confined. Most of the early works concerned systems such as 5CB and 8CB, confined in spherical or cylindrical cavities, in the temperature range corresponding to the bulk isotropic and nematic phases [4–8,10–13]. For large pores, the nematic state persists above the bulk melting temperature. In contrast, under nanometric confinement it has been shown that the orientational order characteristic of the nematic phase still exists below the crystallization temperature, leading to a quenched disorder effect induced by the porous matrices [5–21].

In this work, we report ^{1}H NMR analysis of the liquid crystal MBBA [N-(p-methoxybenzylidene)-p-n-butylaniline; $CH_3{-}O{-}C_6H_4{-}CH = N{-}C_6H_4{-}C_4H_9$] confined in a matrix of silica porous glasses. MBBA is an attractive candidate for such studies owing to its well-established phase diagram [22,23]. Calorimetric measurements have shown that the bulk material exhibits isotropic (I), nematic (N), crystal I (C6), and crystal II (C5) phases upon slow cooling. The quenched effects have also been studied, and it has been shown that a rapid cooling of the nematic phase leads to a glassy nematic liquid crystal (GLC; C0), with a glass transition temperature $T_g = 205\,\mathrm{K}$. Upon slow heating of the GLC, a succession of phases is obtained: solid smectic-like (C1–C2) and crystalline (C3–C4). The confinement effects on a bulk liquid crystal strongly depend on the length scale of the confining material. As extrapolated from a variety of experimental results, the behavior depends on the comparison between the typical length scale of the porous material (d = diameter of pores) and the nematic coherence length (ξ) approximately estimated at 150 Å at the N–I transition for MBBA [24]. To study specifically confinement effects, we have used three different confining lengths of the same porous material (CPG),

treated to minimize surface effects and corresponding to the three cases: $d < \xi$; $d > \xi$; $d \approx \xi$.

The NMR technique has been extensively used to investigate bulk and confined liquid crystals for many years because it provides valuable information on the molecular structure and dynamics by means of spin relaxation analysis. The bulk and confined phases of MBBA were dynamically characterized by studying the temperature dependence of the ^{1}H relaxation times. From the dynamic process probed by NMR and confrontation to the bulk material, we have established conclusions relative to the influence of geometrical confinement on the polymorphism and dynamics of MBBA.

2. EXPERIMENTAL TECHNIQUE

As a porous matrix, we have used controlled porous glasses (CPGs), purchased from CPG Inc. (Fairfield, New Jersey), of nominal pore sizes diameter 337, 156, and 82 Å, referred to as G337, G156, and G82, respectively. This material consists of crushed glass particles with a grain diameter of 40–75 μm. The CPG matrix presents a roughly cylindrical morphology and a narrow pore diameter distribution with 5–10% departures around the average value [2]. Some of their physical properties are given, as supported by the manufacturer, in Table 1. Because the surface of CPG contains hydroxyl groups that may interact with MBBA via hydrogen bonding, the CPGs were chemically treated using hexametyldisilazane according to a procedure described in Ref. [20]. The LC MBBA used in our experiments was synthesized in our laboratory. The molecular length of MBBA is $L = 18$ Å. To fill the pores, the exact amount of MBBA to be used was calculated from the specific pore volume supplied by the manufacturer (Table 1). The porous materials were then saturated by heating the CPG/MBBA mixtures up to the clarification temperature, favoring

TABLE 1 Physical Properties of the Controlled Pore Glasses Used in the Present Study Supported by the Manufacturer (CPG, Inc.)

Label	d[a]	Δd[b] (%)	V[c]	S[d]
G337	337	5.7	0.84	244.5
G156	156	5.8	0.81	90.9
G82	82	7.95	0.37	55

[a]Pore size (Å).
[b]Pore-size distribution (%).
[c]Specific pore volume (cm^3/g).
[d]Specific surface (m^2/g).

the diffusion of MBBA into the pores. The samples were transferred in NMR tubes (5 mm) and sealed to prevent external contamination.

The ^{1}H NMR experiments were carried out on a Bruker ASX100 spectrometer. ^{1}H spectra were obtained by the conventional quadrature fast Fourier transfrom (FFT) method and line-shape simulation of the spectra were performed by standard methods using a computer program. The proton Zeeman spin-lattice relaxation time T_1 was measured with an inversion–recovery pulse sequence $[(\pi, \tau, \pi/2, D_0)_n]$, typically using 12–14 values of τ and a recycle delay $D_0 = 5\ T_1$. At all temperatures, the magnetization relaxation was well fitted using a simple exponential decay with a single time constant T_1 within experimental error. The temperature of the sample was controlled by a conventional Bruker gas-flow system (BVT-2000) over the temperature range 120–350 K, to within ± 0.5 K. Experiments were performed using two different thermal procedures according to previous bulk analysis [22,23]. The sample was first slowly cooled from the isotropic state by lowering the temperature in 5 K intervals to study the phases I $\rightarrow$ N $\rightarrow$ C6 $\rightarrow$ C5. In a second experiment, the sample was quenched below T_g, from room temperature (N), to reach the glassy nematic phase (C0). C0 was then investigated upon cooling from 210 K to 120 K. Upon heating C0 above T_g, a new crystalline phase is obtained after an annealing of several hours at $T = 260$ K. Again, this phase was investigated upon cooling to 120 K. An equilibration delay of 10 min was systematically used before starting the measurements.

3. RESULTS

A. Bulk Analysis

The temperature dependence of the ^{1}H NMR relaxation times of bulk MBBA (N-C6–C5–C0–C4) is represented in Fig. 1 [22]. Within experimental errors, the results are consistent with those previously reported in the literature [25–28]. As seen in Fig. 1, the N-C6 phase transition is related to an important increase of T_1. Upon decreasing the temperature, a continuous T_1 variation is perceived in C6–C5, with a shoulder observed at $T = 200$ K and a minimum at $T = 145$ K. In C0 and C4, the shape of the relaxation curves presents a T_1 minima observed at different temperatures characterizing the solid phases.

Assuming that the motions are thermally activated, the relaxation-rate temperature dependence can be analyzed in terms of the well-known rotational diffusion model (BPP theory; [29,30]):

$$\frac{1}{T_1} = \sum_i C_i\ [g(\omega, \tau_i)]. \tag{1}$$

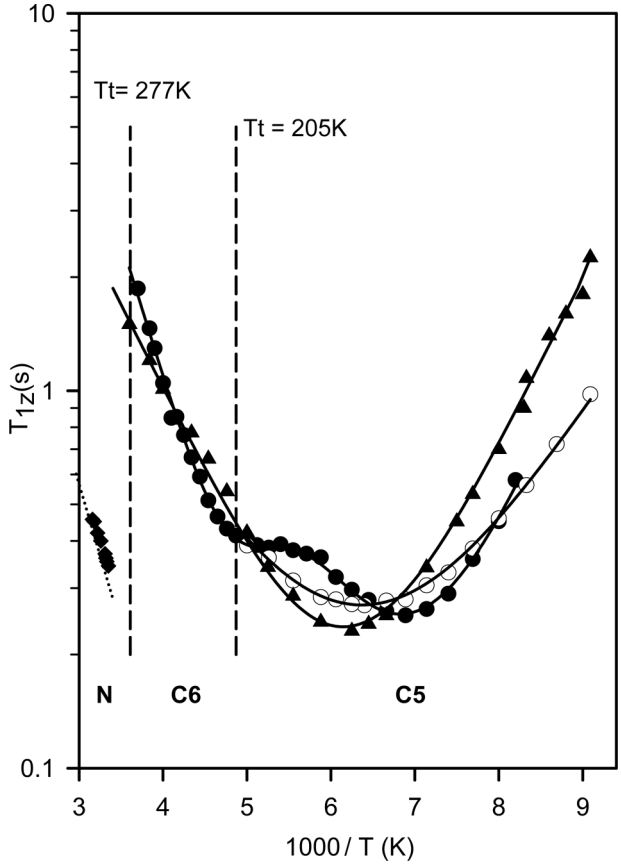

FIGURE 1 Variation of T_1 for bulk MBBA (from Ref. [25]: slow cooling experiments C6–C5 (●), glassy state C0 (○), and crystalline phase C4 (▲). The continuous curves correspond to the best refinement carried out with a BPP model.

The dipolar relaxation constant C_i is given by

$$C_i = \frac{9}{20}\left(\frac{\mu_0}{4\pi}\right)^2 \frac{\gamma^4 \hbar^2}{r_m^6}, \tag{2}$$

where r_m is the appropriate inter proton distance and the other symbols have their usual meaning.

The function g is given by

$$g(\omega, \tau_i) = \left[\frac{\tau_i}{1 + (\omega\tau_i)^2} + \frac{4\tau_i}{1 + (2\omega\tau_i)^2}\right], \tag{3}$$

TABLE 2 Activation Energies (E) and Inverse Frequency Factors (τ_0) Deduced from NMR Analysis of the Solid Phases of Bulk MBBA

Phase	τ_0 (s)	E (KJ/mol)
C6–C5 (τ_1)	$1.5 \cdot 10^{-13}$	15
C5 (τ_2)	$3.9 \cdot 10^{-13}$	9.4
C0	$8.1 \cdot 10^{-12}$	6.26
C4	$1.7 \cdot 10^{-12}$	8.6

where $\omega = \gamma_H B_o$ is the Larmor frequency and the motional correlation times τ_i are assumed to follow an Arrhenius relation:

$$\tau_i(T) = \tau_{o,i} \exp\left(\frac{Ei}{RT}\right). \tag{4}$$

E and τ_0 are respectively the activation energy and the pre-exponential factor characteristic of the invoked motion.

In previous NMR investigations, the low-temperature minima were attributed to the reorientation of methyl groups [25–28]. Under such assumption, the constant C_i is given by [30]:

$$C_i = \frac{9}{20}\frac{n}{N}\left(\frac{\mu_0}{4\pi}^2\right)\frac{\gamma^4 h^2}{r_m^6}, \tag{5}$$

where N is the number of protons in the molecule and n is the number of protons contributing to the relaxation process. The distance $r_m \approx 1.797$ Å is the intramethyl group proton–proton distance.

As displayed in Fig. 1, a good agreement between theoretical and experimental data was obtained assuming that two relaxation processes exits upon a slow cooling experiment (C6–C5: τ_I, τ_{II}), whereas a single one is observed in the other phases. The corresponding motional parameters are given in Table 2. In the crystalline phases (C5, C0, C4), the activation energies of the motion-generating T_1 minimum are found in the range 9–10 KJ/mol, as generally observed for methyl group reorientations in similar systems [25–28,30–32]. In C0, the distribution of environments results in a smaller activation energy (E = 6 KJ/mol).

B. Confined MBBA

Typical ^{1}H NMR line shapes of bulk and confined MBBA (G337) recorded during a slow cooling experiment are shown in Fig. 2. As seen

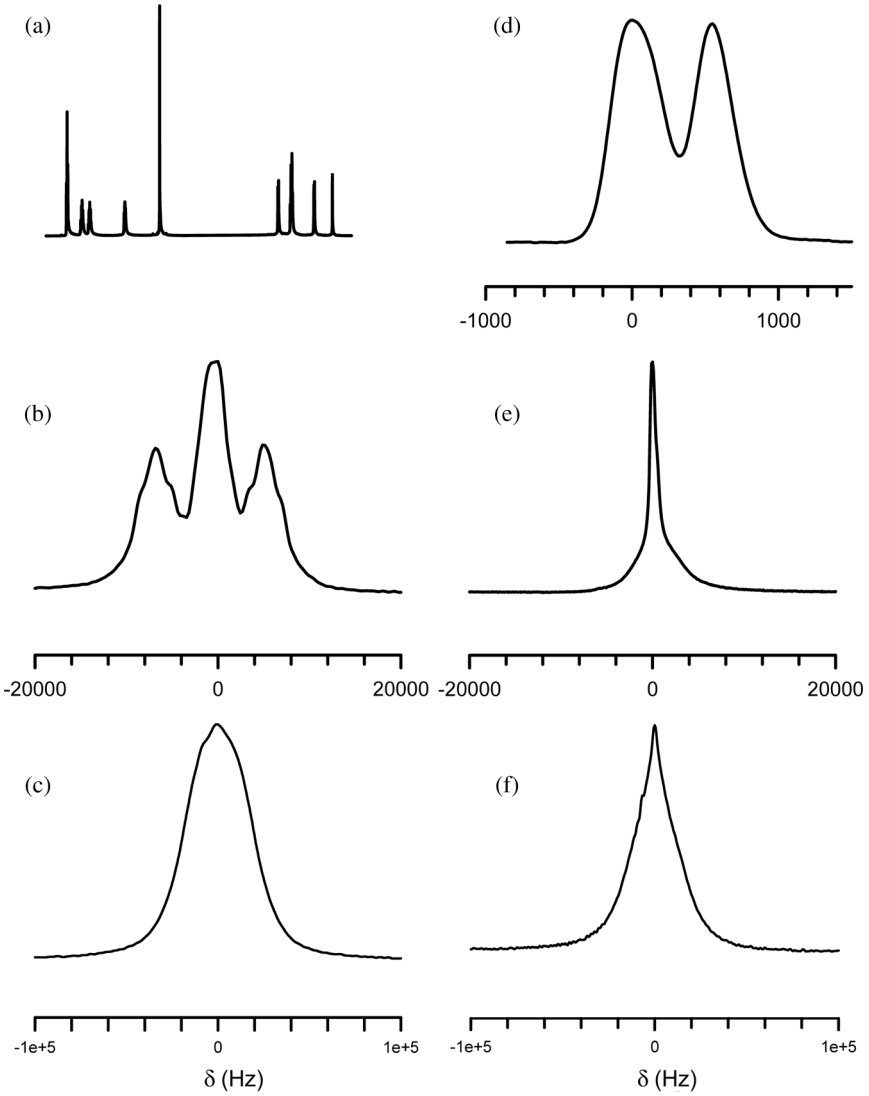

FIGURE 2 Typical NMR spectra of bulk (a, b, c) and confined MBBA [G337 (d, e, f)], recorded in the isotropic (a, d; T = 330 K), nematic (b, e; T = 293 K), and solid (c, f; T = 240 K) phases.

in Fig. 2d, the isotropic G337 NMR spectrum remains broad $\Delta\nu^{\mathrm{CPG337}} \approx 300\,\mathrm{Hz}$ in comparison with the bulk one, $\Delta\nu^{\mathrm{bulk}} = 0.1\,\mathrm{Hz}$ (Fig. 2a). The line-shape is characterized by the presence of two

components with chemical shifts corresponding approximately to the bulk aliphatic and aromatic protons. In the nematic phase, the G337 spectral pattern (Fig. 2e) evolves to an absorption line that does not exhibit any bulk characteristic (Fig. 2b). According to previous LC analysis, this pattern is the one expected for a confined nematic phase [6,7,11,12]. In the crystalline state, a single broad line with a Gaussian and Lorentzian line-shape is observed respectively for the bulk (Fig. 2c) and confined (Fig. 2f) sample. A similar spectral line shape temperature variation is observed for G156 and G82.

The temperature dependence of the ^{1}H NMR relaxation times (T_1, T_2) of confined MBBA (G337, G156, and G82) is represented respectively in Figs. 3–5. As seen in Fig. 2e, a composite NMR line (two-phase

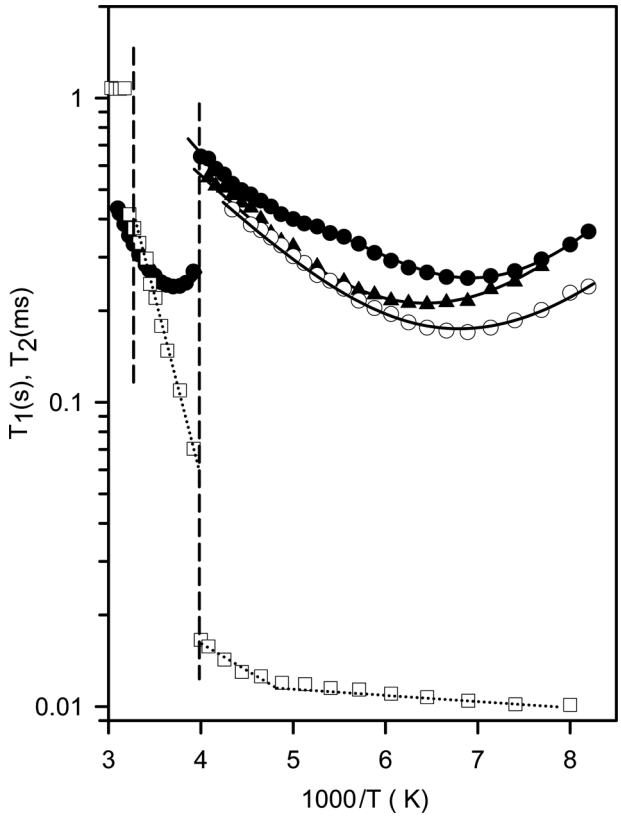

FIGURE 3 Temperature dependence of T_2 (□) and T_1 for MBBA confined in G337: slow cooling experiments (●), glassy state C0 (○), and after heating of the quenched phase (▲). The continuous curves correspond to the best refinement carried out with a BPP model. Dotted lines (T_2) are only guides for the eyes.

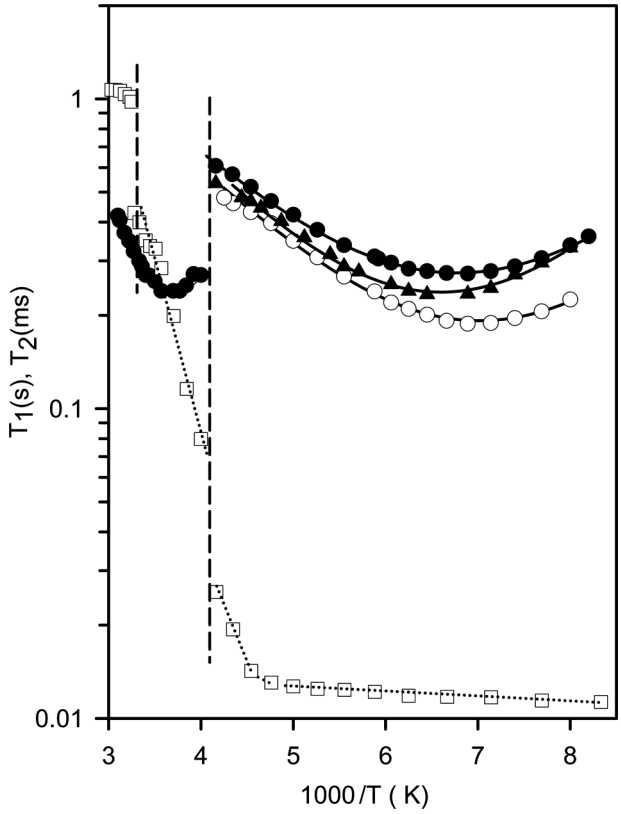

FIGURE 4 Variation of T_2 (□) and T_1 versus $10^3/T(K)$ for MBBA confined in G156: slow cooling experiments (●), glassy state C0: (○), and after heating of the quenched phase (▲). The continuous curves correspond to the best refinement carried out with a BPP model. Dotted lines (T_2) are only guides for the eyes.

system) was observed in the nematic temperature range. According to previous analysis, we have supposed that the narrow line corresponds to molecules in the nematic state located at the center of the pores and the broad line to molecules close to the pores wall. This hypothesis is supported by the fact that upon cooling, the width of the narrow line increases and transforms into a Lorentzian line-shape, merging with the broad-line component below the crystallization temperature. A deconvolution procedure was used for the NMR line width determination. Because we are mainly interested in the phase transformations, we have only reported the temperature variation of the narrow components in Figs. 3–5.

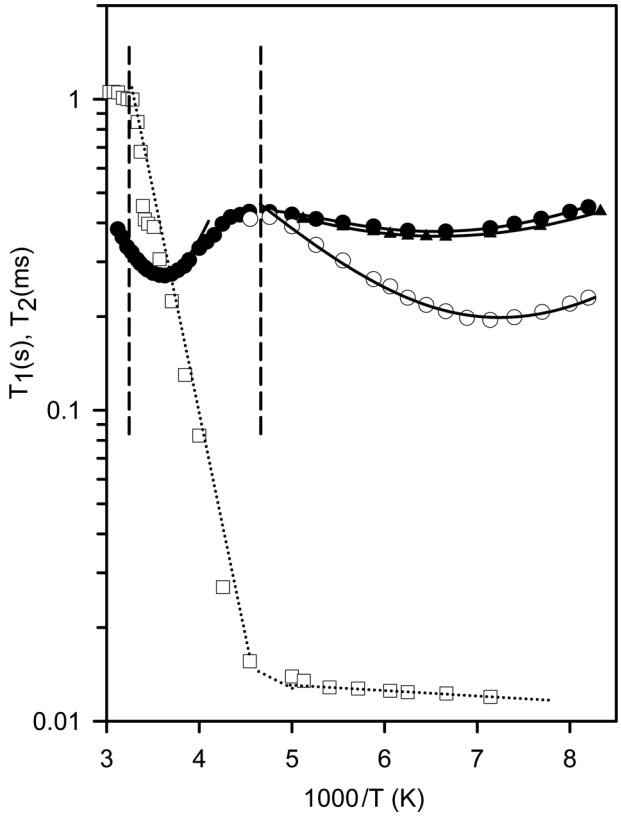

FIGURE 5 Measured values of T_2 (□) and T_1 for MBBA confined in G82: slow cooling experiments (●), glassy state C0: (○), and after heating of the quenched phase (▲). The continuous curves correspond to the best refinement carried out with a BPP model. Dotted lines (T_2) are only guide for the eyes.

As seen in Fig. 3 for G337, T_2 is almost constant in the isotropic phase. At $T \approx 309\,\mathrm{K}$, an important decrease of T_2 related to the $\mathrm{I} \rightarrow \mathrm{N}$ phase transition is observed. Upon decreasing the temperature, a linear variation of T_2 is perceived in the nematic phase followed by a jump related to the crystallization observed at $253 \pm 3\,\mathrm{K}$. Considering T_1, an important difference is observed in the nematic phase, because in G337, T_1 exhibits a minimum at $T \approx 270\,\mathrm{K}$ ($T_1{}^{\mathrm{MIN}} = 250\,\mathrm{ms}$). Generally, a T_1 minimum is impossible to observe in a nematic phase, which exists only in a narrow domain of temperature. In the solid phases, the general T_1 behavior is similar to the bulk, taking into account the depression of the phase-transition temperatures. A T_1 shoulder is

perceived at $T \approx 190\,\mathrm{K}$ ($T_1^{\mathrm{MIN}} = 380\,\mathrm{ms}$) and a second minimum is observed at $T \approx 145\,\mathrm{K}$ ($T_1^{\mathrm{MIN}} = 250\,\mathrm{ms}$). From the slope of the relaxation curves, we have obtained $E = 6.5\,\mathrm{KJ/mol}$ and $5.9\,\mathrm{KJ/mol}$, respectively, for the high and low temperature motion process. In C0, a minimum is observed at $T \approx 147\,\mathrm{K}$ ($T_1^{\mathrm{MIN}} = 170\,\mathrm{ms}$). As seen in Fig. 3, both the depth and the temperature of this minimum are different from those observed in C5, and the existence of a glassy state in G337 is confirmed by NMR. After a recrystallization in C4, a new minimum is reached at $\mathrm{T} \approx 156\,\mathrm{K}$ ($T_1^{\mathrm{MIN}} = 210\,\mathrm{ms}$).

The temperature dependence of the proton relaxation times of MBBA confined in G156 is represented in Fig. 4. In G156, the I–N phase transition is detected by a T_2 jump at $T \approx 305\,\mathrm{K}$ and a T_1 minimum is observed in the nematic phase at $T \approx 266\,\mathrm{K}$ ($T_1^{\mathrm{MIN}} = 232\,\mathrm{ms}$). Upon decreasing the temperature, a T_1 gap related to the crystallization is observed at $T = 245\,\mathrm{K}$. In the solid phase, T_2 displays a constant value, and T_1 exhibits a minimum at $T \approx 148\,\mathrm{K}$ ($T_1^{\mathrm{MIN}} = 274\,\mathrm{ms}$). The disappearance of the shoulder observed for both the bulk and G337 samples suggests, in agreement with X-ray investigations, that MBBA is unable to crystallize in C6 when the pore size becomes too small ($d < 337\,\mathrm{\AA}$) [23]. From this hypothesis, the crystal phase corresponds to C5, and we have found $E = 4.86\,\mathrm{KJ/mol}$ for G156. As seen in Fig. 4, a single and different minimum is observed in C0 at $T \approx 143\,\mathrm{K}$ ($T_1^{\mathrm{MIN}} = 192\,\mathrm{ms}$) and after crystallization in C4 at $T \approx 151\,\mathrm{K}$ ($T_1^{\mathrm{MIN}} = 238\,\mathrm{ms}$).

In G82 ($d < \xi$), the temperature dependence of the proton relaxation times appears very different, indicating a more important confinement effect (Fig. 5). At temperatures greater than $T \approx 301\,\mathrm{K}$, the system is in an isotropic state, and T_2 displays a constant value. Upon slow cooling, a continuous temperature variation of the relaxation times (T_2 and T_1) is observed between $T = 300\,\mathrm{K}$ and $T = 120\,\mathrm{K}$. In the nematic state, T_2 varies almost linearly. At $T \approx 220\,\mathrm{K}$, a plateau characteristic of a solid phase is reached. This behavior confirms that for the microporous confinement, crystallization exits even if no heat capacity peak is detected by very slow cooling calorimetry experiment ($0.1\,\mathrm{K/min}$ [22]). As for the other samples, there exists a first minimum in the nematic phase at $T \approx 274\,\mathrm{K}$ ($T_1^{\mathrm{MIN}} = 270\,\mathrm{ms}$) and a second minimum in the crystalline phase at $T \approx 152\,\mathrm{K}$ ($T_1^{\mathrm{MIN}} = 362\,\mathrm{ms}$). The depth of the solid phase minimum is substantially greater than those measured for the same phase in the other samples. As a result, the corresponding activation energy becomes very small: $E = 3.2\,\mathrm{KJ/mol}$. In contrast, the T_1 behavior of C0 is similar to those observed for the other samples: $E = 5\,\mathrm{KJ/mol}$, and a single minimum is perceived ($T \approx 138\,\mathrm{K}$; $T_1^{\mathrm{MIN}} = 198\,\mathrm{ms}$) in the range of those observed for the other

TABLE 3 Activation Energies (E) and Inverse Frequency Factors (τ_0) Deduced from NMR Analysis of Confined MBBA

Sample	Phase	τ_0 (s)	Ea (KJ/mol)	r_{ij} (Å)
G337	NEMATIC	$8.0 \cdot 10^{-13}$	15.7	1.84
	C6–C5 (τ_1)	$3.2 \cdot 10^{-11}$	10.3	2.35
	C5 (τ_2)	$3.7 \cdot 10^{-12}$	6.6	1.87
	C0	$1.1 \cdot 10^{-11}$	5.5	1.75
	C4	$1.1 \cdot 10^{-11}$	5.82	1.80
G156	NEMATIC	$6.1 \cdot 10^{-13}$	16.5	1.85
	C5 (τ_2)	$1.8 \cdot 10^{-11}$	4.86	1.88
	C0	$1.3 \cdot 10^{-11}$	5.16	1.78
	C4	$9.2 \cdot 10^{-12}$	5.88	1.84
G82	NEMATIC	$6.2 \cdot 10^{-13}$	16.9	1.88
	C5 (τ_2)	$8.14 \cdot 10^{-11}$	3.2	2.00
	C0	$1.26 \cdot 10^{-11}$	5.0	1.79

confined and bulk samples. Upon heating C0, a radically different behavior is observed in G82 because T_1 was found, within experimental errors, identical to the results obtained under a slow cooling experiment. We concluded that in G82, the same crystalline phase is reached under a slow cooling experiment and upon heating the sample from C0.

The best fits obtained using Eq. (1), assuming a composite motion with two processes in G337 [τ_I (C6) and τ_{II} (C5)] and a single correlation time related to end-group motions in the other phases, are represented as solid lines in Figs. 3–5. The corresponding parameters are given in Table 3.

4. DISCUSSION

A phase diagram for the transition temperatures versus inverse pore-size diameter, obtained by NMR and DSC (from Ref. [23]), is presented in Fig. 6. From a comparison of the results, there is experimental evidence that the confinement induced a decrease of the transition temperatures. This behavior, which is consistent with many experimental analyses of confined LCs, is the one expected when finite size effects prevail [33]. Moreover, a linear variation (with different slopes) of the depression, versus inverse pore diameter, is observed for all the phase transitions investigated. As a result, the existence range of the nematic domain increases when the pore size is reduced. According to our results, for $d < 60$ Å, no crystallization of MBBA would be observed upon cooling.

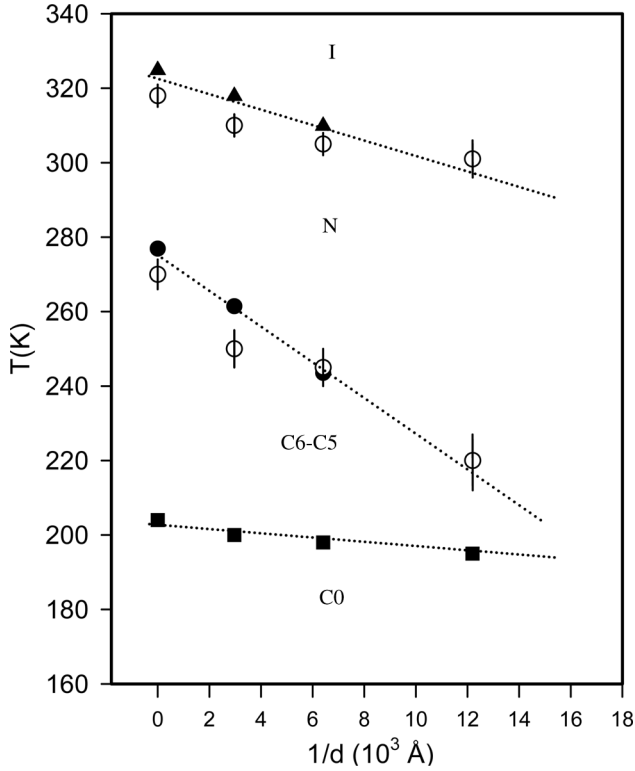

FIGURE 6 Comparison of the phase-transition temperatures obtained by DSC (T_{NI} (▲), T_{NC6} (●), Tg (■); from Ref. [23]), and NMR (○) for bulk and confined MBBA.

From our NMR investigation, we have concluded that a nematic phase still exists in G82 unlike no thermal event observed by DSC [23]. As seen in Fig. 6, the G82 phase-transition temperatures deduced from NMR are fully consistent with the linear prediction obtained from the Gibbs–Thomson equation. In G82, which corresponds roughly to 4 molecular diameters, the relation ($d = 82\,\text{Å} < \xi = 150\,\text{Å}$) implies the existence of both important size and surface effects. Consequently, the installation of a nematic local order seems difficult to understand. A possible explanation is that the phase transition determined by NMR corresponds to bulk-like orientational ordering in porous region, like interpore channels, of a size larger than the mean pore size given by the manufacturer. The role played by the pore geometry in the confined material appears crucial and the CPG

samples, which are characterized by a distribution of orientation, are not the ideal material to get insight into this problem.

In a nematic phase, it is well-known that the proton spin-lattice relaxation results from the modulation of dipolar interactions and is expressed as the sum of three mechanisms [34–36]:

$$\frac{1}{T_1} = \left(\frac{1}{T_1}\right)_{\mathrm{SD}} + \left(\frac{1}{T_1}\right)_{\mathrm{ODF}} + \left(\frac{1}{T_1}\right)_{\mathrm{R}}. \tag{6}$$

$(T_1^{-1})_{\mathrm{SD}}$ corresponds to translational self-diffusion, $(T_1^{-1})_{\mathrm{ODF}}$ to nematic order director fluctuations, and $(T_1^{-1})_{\mathrm{R}}$ to rotational reorientations. According to field-cycling analysis, translational self-diffusion is the dominant mechanism of relaxation in the MHz regime, whereas the other contributions are effective in the low-frequency regime [34–36]. From NMR investigation, it has been shown that the SD mechanism gives a T_1 minimum proportional to the static field according to the relation [37]:

$$\frac{T_{1\mathrm{MIN}}}{\omega} = 4.0 \cdot 10^{-10}\, s^2 \tag{7}$$

This relation is consistent with the experimental minimum observed in the nematic phase of the confined samples; for example, at 100 MHz in G337, we have found $T_{1,\mathrm{MIN}}^{\mathrm{calc}} = 0.251\,\mathrm{s} \approx T_{1,\mathrm{MIN}}^{\mathrm{Exp}} \approx 0.256\,\mathrm{s}$. As seen in Figs. 3–5, taking advantage of the occurrence of minima in the nematic phase, the experimental data are well described by assuming a BPP model for the description of this mechanism [Eq. (1)]. As a result, E was found to increase from 13 KJ/mol (bulk) to 15.7–16.9 KJ/mol for the confined samples. However, only a weak variation of the correlation times is observed when the degree of confinement increases; at $T = 293\,\mathrm{K}$, we found: $\tau_{(\mathrm{G337})} = 5 \cdot 10^{-10}\,\mathrm{s}$, $\tau_{(\mathrm{G156})} = 5.3 \cdot 10^{-10}\,\mathrm{s}$, and $\tau_{(\mathrm{G82})} = 6.3 \cdot 10^{-10}\,\mathrm{s}$ using the parameters of Table 3.

As for the bulk, a glassy state is reached when MBBA is confined in CPG. Again, a linear decrease of T_g, as a function of the inverse pore diameter, has been observed by calorimetry (Fig. 6 [23]). However, as seen in Fig. 6, the extent of the depression is smaller (ΔT_g (max) $\approx 10\,\mathrm{K}$) than for the other phase transition. This small negative shift is fully consistent with the small enhancement of the dynamics observed at a given temperature by NMR: $E = 5.5$–$5\,\mathrm{KJ/mol}$ and at $T = 190\,\mathrm{K}$: $\tau = 3.5$–$3 \cdot 10^{-10}\,\mathrm{s}$, respectively, in G337 and in G82 (Table 3). A possible interpretation of this variation is provided by the concept of cooperativity length (ζ) and the Adam–Gibbs model [15,16,38]. From a qualitative point of view, and assuming that the cooperativity length increases with decreasing temperature, a shift of T_g to the lower

temperatures is expected in restricted geometries when $d < 2\zeta$ [15,16]. For a quantitative estimation, we have used the method described in Ref. [16] where it is shown that the extrapolated value corresponding to $\Delta T_g = 0$ gives approximately $\zeta/2$. Using the same model, we have measured $\zeta \leq 25\,\text{nm}$ for MBBA. For comparison, the ζ at T_g reported in the literature are of few nanometers for glass-forming liquids [15,16].

When the crystallization of confined MBBA occurs, the relaxation curves were well described using the BPP model [Eq. (1)]. As seen in Table 3, an important decrease of the activation energies is observed when the pore size decreases. In G337, the residence time of the bulk molecular motion (τ_2) is enhanced by almost one decade; at $T = 250\,\text{K}$, we have obtained $\tau_{(\text{bulk})} = 2 \cdot 10^{-10}\,\text{s}$, $\tau_{(\text{G337})} = 4 \cdot 10^{-9}\,\text{s}$. This motion is then strongly sensitive to the confinement effect, and for $d < 337\,\text{Å}$ this contribution completely disappears. Consequently there exist more important dynamics variations in the solid phases upon increasing the confinement. According to this result, it was not possible to use the NMR dynamical parameters to identify, by comparison with the bulk analysis, the different phases of confined MBBA. Considering the low-temperature motion, it is difficult to explain the large dispersion in the activation energies of Table 3, because the barrier hindering methyl rotation is supposed to be of intramolecular origin and must be therefore relatively independent of the phase considered. For example, the shallow T_1 minimum in G82 gives rise to an activation energy lower than values generally admitted for the same motion in similar compounds. These considerations suggest a complex dynamical behavior resulting from the co-existence of poorly crystallized and amorphous regions, with this effect being more pronounced in G82. In G337, this hypothesis is fully consistent with the strong difference observed in Figs. 1c and 1f, the latter indicating the existence of different dynamical populations. This situation is quite likely to occur because the pore structure gives rise to several environments related, for example, to molecules that are located close to the pore surface and to molecules located at the center of the pores. The molecules located close to the pore surface are in a different state, giving rise to different motional parameters. As a result, the description of the molecular motion with a BPP model and a single correlation time leads to some unrealistic parameters. In this case, another method to describe the relaxation-rate temperature dependence consists in introducing a distribution of correlation times. In the following, we have used a Cole–Cole distribution, characterized by its symmetrical shape with respect to the T_1 minimum as it is observed in Figs. 3–5. The Cole–Cole distribution is defined by [39,40]

$$\theta_{CC} = \frac{1}{2\pi}\sin(\beta\cdot\pi)\left[\frac{1}{\cosh(\beta\cdot z)+\cos(\beta\cdot\pi)}\right], \tag{8}$$

where β ($0 < \beta \leq 1$) is the distribution width, $\beta = 1$ is the limit of a single correlation time, $\beta = 0$ is an infinitely broad distribution, and the variable $z = \ln(\tau/\tau_{\max})$, where $\tau_{\max}$ is the correlation time corresponding to the maximum of θ_{CC} [40].

To account for a Cole–Cole correlation time distribution, the NMR rate expression [Eq. (1)] is used with [40]

$$g_{CC}(\omega,\tau,\beta) = \left(\frac{(\omega\tau)^{\beta}\sin(\beta\pi/2)}{\omega(1+(\omega\tau)^{2\beta}+2(\omega\tau)^{\beta}\cos(\beta\pi/2)} + 4\frac{(2\omega\tau)^{\beta}\sin(\beta\pi/2)}{2\omega(1+(2\omega\tau)^{2\beta}+2(2\omega\tau)^{\beta}\cos(\beta\pi/2)}\right). \tag{9}$$

The experimental data were then fitted with this model by starting the fits with the bulk parameters. The best fit corresponding parameters are given in Table 4. The calculated curves (not represented in Figs. 3–5 for clarity) are superimposed with those obtained by the BPP model. As seen in Table 4, the best-fitted curves were obtained with the bulk activation energies. The parameters τ_0 and β depend on the phase and pores diameter. Although we have considered only a single frequency relaxation measurement, this model allows an interesting comparison between the bulk and confined dynamical parameters. To compare the results, in Fig. 7 we have represented θ_{CC} for each investigated phases (at $T = 150\,\mathrm{K}$), together with the distribution parameter β versus inverse pore radius $1/d$. In C0, β varies linearly from 0.98 to 0.87 when the confinement

TABLE 4 NMR Fitted Parameters of Confined MBBA Obtained Using a Cole–Cole Relaxation Time Distribution

Sample	Phase	τ_0 (s)	Ea (KJ/mol)	r_{ij} (Å)	β
G337	C5	$4.3\cdot10^{-13}$	9.4	1.75	0.76
	C0	$6.0\cdot10^{-12}$	6.26	1.73	0.98
	C4	$1.2\cdot10^{-12}$	8.6	1.70	0.80
G156	C5	$4.3\cdot10^{-13}$	9.4	1.70	0.6
	C0	$4.9\cdot10^{-12}$	6.26	1.73	0.90
	C4	$1.2\cdot10^{-12}$	8.6	1.71	0.72
G82	C5	$7.0\cdot10^{-13}$	9.4	1.70	0.45
	C0	$4.5\cdot10^{-12}$	6.26	1.73	0.87

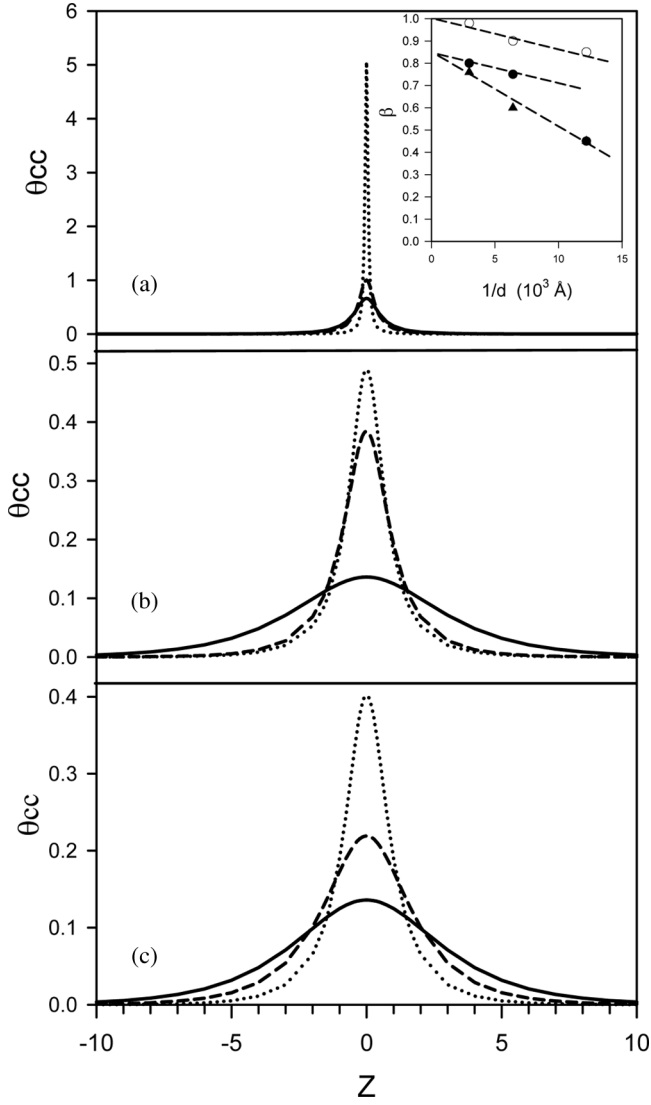

FIGURE 7 Plot of the Cole–Cole distribution of correlation times at 150 K for the: a) quenched samples (C0), b) heating of C0 (C4), and c) slow cooling experiment (C5) of MBBA confined in G337 (dotted line), G156 (dashed lines), and G82 (solid lines). The inset represents the variation of the distribution parameter β at T = 150 K as a function of the inverse pores diameter for C5 (●), C0 (○), and C4 (▲).

increases, revealing a relatively narrow distribution. In the crystalline phases, more significant variations of β are observed (β varies from 0.8 to 0.45). Moreover, as seen in Fig. 7, we have observed a linear dependence of β and different slopes depending of the investigated phase. Upon a slow cooling experiment (C5), the β parameters related to the different pore size are aligned. Then we concluded that a slow cooling experiment leads to a crystallization in C5 independent of the pore size. The same β parameter is obtained upon heating a G82 quenched sample (C0). We concluded that in G82, MBBA crystallizes in C5 upon heating instead of C4–C3 as observed for the other pore sizes. As a consequence, the phase diagram of confined MBBA is different from the bulk, particularly when $d \leq 82\,\text{Å}$. Because we have found that β depends on the phase investigated, the distribution is not determined only by geometrical considerations. However, these results need to be confirmed by complementary NMR investigation at different frequencies and by other techniques such as dielectric relaxation.

5. CONCLUSION

The spatial confinement has a strong influence on the polymorphism and dynamics of MBBA. In CPG we have shown that the temperatures of the phase transitions are linearly depressed when the confinement increases and that above $d \approx 60\,\text{Å}$, a crystallization of MBBA is expected under a slow cooling experiment. For the largest pores, the bulk phase diagram is still valid. In contrast, when the pore size becomes smaller, important modifications are observed, and our results revealed in G82 that the same phases are reached under a slow cooling from room temperature and upon heating a quenched sample. In the nematic phase, the confinement, by depressing the crystallization temperature, allows us to determine the molecular motion parameters relative to a mechanism attributed to self-diffusion. This motion was found to be weakly influenced by the confinement. In the solid phases, a reduction of the activation energies occurred when the pore size was decreased. To account for this behavior, we have introduced a distribution of correlation times, and we have found a linear variation of the distribution parameter versus inverse pore diameter in the crystalline phase. The glassy state of confined MBBA appears less dynamically altered than in the other solid phases. Because a confined sample can be quenched more easily, the confinement offers a new method to get an insight into the dynamical parameters of quenched LCs.

REFERENCES

[1] Gelb, L. D., Gubbins, K. E., Radhakrishman, R., & Sliwinska-Bartkowiak, M. (1999). *Rep. Prog. Phys.*, *62*, 1.
[2] Booth, H. F. & Strange, J. H. (1998). *Mol. Phys.*, *93*, 263.
[3] Aksmes, D. W. & Kimtys, L. (1998). *Magn. Res. Chem.*, *36*, 747.
[4] Batalla, B., Sinha, G., & Aliev, F. M. (1999). *Mol. Cryst. Liq. Cryst.*, *331*, 121.
[5] Iannachione, G. S., Qian, S., Finotello, D., & Aliev, F. M. (1997). *Phys. Rev. E*, *56*, 554.
[6] Kralj, S., Zidansek, A., Lahajnar, G., Musevic, I., Zumer, S., Blinc, R., & Pintar, M. M. (1996). *Phys. Rev. E*, *53*, 3629.
[7] Iannachione, G. S., Crawford, G. P., Qian, S., Doane, J. W., & Finotello, D. (1996). *Phys. Rev. E*, *53*, 2402.
[8] Schuller, J., Richert, R., & Fisher, E. W. (1975). *Phys. Rev. B*, *52*, 15232.
[9] Dosseh, G., Xia, Y., & Alba-Simionesco, C. (2003). *J. Phys. Chem. B*, *107*, 6445.
[10] Wasyluk, L., Peplinska, B., Klinowski, J., & Jurga, S. (2002). *Phys. Chem. Chem. Phys.*, *4*, 2392.
[11] Gnatyuk, I., Puchkovska, G., Chashechnikova, I., Nozirov, F., Jurga, S., & Peplinska, B. (2004). *J. Mol. Struct.*, *700*, 183.
[12] Han, J. W. (1998). *J. Korean Phys. Soc.*, *33*, 714.
[13] Leon, N., Korb, J. P., Bonalde, I., & Levitz, P. (2004). *Phys. Rev. L.*, *92*, 195504.
[14] Lusceac, S. A., Koplin, C., Medick, P., Vogel, M., Brodie-Linder, N., Lequellec, C., Alba-Simionesco, C., & Rossler, E. A. (2004). *J. Phys. Chem. B*, *108*, 16601.
[15] Pissis, P., Daoukaki-Diamanti, D., Apekis, L., & Christodoulidis, C. (1994). *J. Phys. Condens. Matter*, *6*, L325.
[16] Pissis, P., Kyritis, A., Barut, G., Pelster, R., & Nimtz, G. (1998). *J. Non-Cryst. Solids*, *235–237*, 444.
[17] Patkowski, A., Ruths, T., & Fisher, E. W. (2003). *P. R. E.*, *67*, 021501.
[18] Jackson, C. L. & Mc Kenna, G. B. (1991). *J. Non-Cryst. Solids*, *131–133*, 221.
[19] Jackson, C. L. & Mc Kenna, G. B. (1996). *Chem. Mat.*, *8*, 2128.
[20] Jackson, C. L. & Mc Kenna, G. B. (1990). *J. Chem. Phys.*, *93*, 9002.
[21] Feldman, D. E. (2000). *Phys. Rev. L.*, *84*, 4886.
[22] Pepy, G., Fouret, R., More, M., & Rosta, L. (1989). *Liq. Cryst.*, *5*, 571.
[23] Mansare, T., Gors, C., & More, M. (1998). *J. Therm. Anal.*, *51*, 823.
[24] Chu, B., Bak, C. S., & Lin, F. L. (1972). *Phys. Rev. L.*, *28*, 111.
[25] Decressain, R., Cochin, E., Mansare, T., & More, M. (1998). *Liq. Cryst.*, *25*, 517.
[26] Dolganov, V. K., Pocsik, I., & Rosta, L. (1993). *Liq. Cryst.*, *14*, 1895.
[27] Kumagai, M., Soda, G., & Chihara, H. (1981). *J. Magn. Reson.*, *42*, 28.
[28] Froix, M. & Pochan, J. (1978). *Mol. Cryst. Liq. Cryst.*, *46*, 47.
[29] Bloembergen, N., Purcell, E. M., & Pound, R. V. (1948). *Phys. Rev.*, *73*, 679.
[30] Andrew, E. R. & Peplinska, B. (1990). *Mol. Phys.*, *70*, 505.
[31] Beckmann, P. A., Happerset, L., Herzog, A. V., & Tong, W. M. (1991). *J. Chem. Phys.*, *95*, 828.
[32] Czaplicki, J., Pislewski, N., & Glinka, R. (1990). *J. Magn. Res.*, *88*, 146.
[33] Alba-Simionesco, C., Dosseh, G., Dumont, E., Frick, B., Geil, B., Morineau, D., Teboul, V., & Xia, Y. (2003). *Eur. Phys. J. E*, *12*, 19.
[34] Graf, V., Noack, F., & Stohrer, M. (1977). *Z. Nat.*, *32a*, 61.
[35] Reinhart, K. F., Seeliger, R., Graf, V., & Noack, F. (1979). *J. Physique*, *40*, 199.
[36] Blinc, R., Vilfan, M., & Rutar, V. (1975). *Sol. Stat. Comm.*, *17*, 171.
[37] Ukleja, P. & Doane, J. W. (1978). *Chem. Phys. Lett.*, *53*, 105.
[38] Adam, G. & Gibbs, J. H. (1965). *J. Chem. Phys.*, *43*, 139.
[39] Noack, F. (1971). *NMR Basic Principles and Progress*, Springer: New York.
[40] Beckmann, P. A. (1988). *Phys. Rep.*, *171*, 85.